Parametric Study of Flutter Derivatives of Bridge Cross Sections and Their Implications on the Aeroelastic Stability of Flexible Bridges

by

Partha P. Sarkar[1], Luca Caracoglia[2], Fred L. Haan, Jr.[3]

ABSTRACT

Results of various experimental flutter derivative extraction techniques are compared in this paper. The motivation for this work emerged from the U.S.-Japan Benchmark Study on Bridge Flutter Derivatives that Iowa State University (ISU) in the US and the Public Works Research Institute (PWRI) in Japan initiated in 2002. In the first part, a systematic analysis of laboratory results was conducted; this included free and forced-vibration wind tunnel methods, which are routinely employed by researchers or designers. Data from US and Japanese laboratories were compared considering both streamlined and bluff deck sections. In the second part, a sensitivity study was performed to examine the implications of the perceived dissimilarities among flutter-derivative data sets on the aeroelastic instability of long-span bridges. It was found that flutter derivative uncertainty did not directly relate to flutter velocity. Flutter derivative uncertainties were estimated anywhere between negligibly small values to as much as 50%. The resulting flutter velocities, however, depended heavily on the type of bridge and mode of flutter. Flutter velocity uncertainty values were estimated from as small as 5% to as large as 30% depending on various conditions.

KEYWORDS: bridge aerodynamics, free and forced vibration, bridge flutter-derivative benchmark study, flutter speed calculation.

1.0 INTRODUCTION

The motivation for this work emerges from the U.S.-Japan Benchmark Study on Bridge Flutter Derivatives that Iowa State University (ISU) in the US and the Public Works Research Institute (PWRI) in Japan initiated in 2002. Five bridge cross sections were proposed to be tested: (1) Rectangle (2:1 section), (2) Π-section (or edge girder section), (3) Streamlined Box Girder, (4) Slotted Box Girder, and (5) Original Tacoma Narrows. Sarkar et al. (2006) reported good comparison between the ISU free vibration data and PWRI forced vibration data (Sato, 2004) of all the eight flutter derivatives of the Streamlined Box Girder and Slotted Box Girder sections associated with their vertical-torsional motion except for some minor discrepancies.

Section model tests of the decks of long-span bridges have long been conducted as part of the design process for new bridges. Over the years, numerous methods have been developed to extract the required aeroelastic and aerodynamic parameters from the tests. Although the technical implementation of each method can vary widely, all methods can be grouped into two broad categories—those involving free vibration tests and those involving forced vibration tests. Both methods have advantages for different scenarios. Free vibration systems do not force any prescribed motion on the model but rather allow the fluid structure interaction to drive the motion. Forced

[1] Professor and Wilson Chair, [3] Assistant Professor
Wind Simulation and Testing Laboratory, Department of Aerospace Engineering, Iowa State University, 2271 Howe Hall, Room 1200, Ames, IA 50011-2271 USA

[2] Assistant Professor, Department of Civil and Environmental Engineering, Northeastern University, 360 Huntington Avenue, Boston, MA 02115 USA

vibration systems, however, are sometimes able to deal with cases involving larger reduced velocities or higher turbulence intensities that would be very difficult with free vibration tests.

In the past, very few studies have been conducted to examine the equivalence of results from free and forced methods. The work described here relates to an effort to compare the results of forced and free vibration testing within the same laboratory as well as two different laboratories. This paper focuses on two rectangular sections and provides comparison between ISU data set with another data set from Japan (Matsumoto, 1996). Many researchers in the past have suspected flutter derivatives to be amplitude dependent but none has explored it completely. One degree-of-freedom (DOF) free-vibration tests in heaving motion were conducted for up to three different initial amplitudes. The results were compared with each other and with those from Japan. Recent comparison of flutter derivatives of a particular streamlined deck that were obtained using the forced vibration method (Haan, 2000) with those from free vibration (Gan Chowdhury and Sarkar, 2003) showed some differences at ISU. This motivated us to perform an uncertainty analysis to estimate the variation of flutter derivatives obtained from this forced-vibration method. Since this method uses phase angle between displacement and force or moment to calculate the flutter derivatives and the phase angle depends on many factors including instrumentation, sampling rate, and filters used, it was decided to estimate the errors that could arise as a result of these factors. Lastly, flutter-speed predictions for long-span bridges of various spans were considered in terms of the variation in flutter derivatives due to different methods, laboratories, and amplitudes. Flutter speeds corresponding to single-mode or multi-mode flutter for a streamlined and a rectangular section were estimated using a range of flutter derivatives obtained at ISU and from Japan.

2.0 EXPERIMENTAL FACILITIES

A test section was built to accommodate section model testing in the Bill James Wind Tunnel (see Figure 1) at Iowa State University's Wind Simulation and Testing Laboratory. The Bill James tunnel has a 0.91m by 0.76m test section and an 80m/s maximum velocity. Section models that are suspended by linear springs slide on guide rails with extremely low friction air bearings. For free vibration testing, models are free to move with three degrees of freedom (DOFs)—plunge, pitch, and sway. Figure 2 shows a picture of the model in this suspension system; further details can be found in Sarkar et al. (2004). For forced vibration tests, only pitching and plunging DOFs are employed. The forced vibration excitation system is mounted on a frame above the test section (see Figures 1 and 2). Rods extend into the test section to drive the model motion. These rods are removed for free vibration tests. The initial displacements for the free vibration tests are accomplished using a setup of electromagnets, strings and pulleys (Figure 3). Forced vibration tests require lift and moment to be measured simultaneously with vertical or angular position. In this case, lift and moment were calculated using pressure measurements on the models. The top and bottom surfaces of the models were instrumented with 16 pressure taps each. Pressures were measured with an electronic pressure scanner and the signals were corrected for the dynamic effects of the tubing. More details can be found in Section 4.0.

The results of testing one streamlined box girder model (B1) with semi-circular fairings for the edges, as shown in Figure 4, are presented in this paper. The first test involved B1 that had a B/D ratio (width to depth) of 14.3 and a length of 0.6 m, respectively. This model was used in tests at ISU that compared free and forced vibration methods of flutter derivative extraction. Two other models with bluff cross sections, "R2_1" and "R5_1," as shown in Figure 5, were also tested at ISU. These models were rectangle box girders with a B/D = 2 (R2_1) and B/D = 5 (R5_1). Each model had a span of 0.533 m. Two Plexiglas end plates were used to reduce aerodynamic end effects for all models.

For comparison purposes and within the scope of the benchmark study, results from another laboratory are included in this paper. Matsumoto (1996) extracted flutter derivatives with a forced vibration system. In this system, the unsteady aerodynamic pressures acting on a section model were measured in two separate one-DOF tests. The aerodynamic forces and moments were obtained by integrating these pressures and four aerodynamic derivatives were estimated from each test using these aerodynamic forces or moments and forcing displacements measured at the same time.

3.0 ANALYTICAL APPROACH OF EACH METHOD

The methods for free vibration and forced vibration analysis employed for this study used the following formulation for the aeroelastic forces acting on a bridge deck:

$$L_{ae} = \frac{1}{2}\rho U^2 B\begin{bmatrix} KH_1^*\frac{\dot{h}}{U} + KH_2^*\frac{B\dot{\alpha}}{U} \\ + K^2 H_3^*\alpha + K^2 H_4^*\frac{h}{B}\end{bmatrix} \quad (1)$$

$$M_{ae} = \frac{1}{2}\rho U^2 B^2\begin{bmatrix} KA_1^*\frac{\dot{h}}{U} + KA_2^*\frac{B\dot{\alpha}}{U} + \\ K^2 A_3^*\alpha + K^2 A_4^*\frac{h}{B}\end{bmatrix}$$

where B is the bridge deck width, U is the mean wind velocity, ρ is the air density, K is the reduced frequency and h and α represent heaving and pitching displacements, respectively (with the dot representing a time derivative). The reduced frequency K is defined as $\omega B/U$ where ω is the frequency of vibration. The reduced frequency is proportional to the reciprocal of the reduced velocity, U_r, which is defined as U/nB where n is the frequency of oscillation in Hz ($\omega=2\pi n$).

The free vibration testing of the present work employs a new system identification method (Iterative least squares method or ILS method) that can efficiently extract up to eighteen flutter derivatives associated with three-DOF motion of a section model. This identification technique (Gan Chowdhury and Sarkar, 2003, 2004) uses experimentally obtained free-vibration displacement time histories generated by a section model supported by a three-DOF elastic suspension system (Sarkar et al., 2004) inside a wind tunnel test section. The ILS method extracts the flutter derivatives by using an iterative technique to identify the stiffness and damping matrices that are associated with the equations of motion at a given wind speed. The ILS method can also be applied to fewer DOF (two or one), if needed, by appropriately restraining the section model to vibrate along certain DOF(s). In fact, it is recommended that performing three different sets of two-DOF testing, namely, vertical-torsional, vertical-lateral, and lateral-torsional, instead of three-DOF testing, would be more efficient procedure for accurate extraction of all the eighteen derivatives. In this paper, results from one-DOF testing for the rectangular sections R2_1 and R5_1 for three initial amplitudes, A=9 mm, 17 mm and 26 mm, two cases of two-DOF testing (vertical-torsional and lateral-vertical) of B1 (Gan Chowdhury and Sarkar, 2003, 2004) and one case of one-DOF forced vibration testing (torsional) of B1 are presented. Details of the identification technique (ILS method) and experimental procedure for the free vibration method can be found in Gan Chowdhury and Sarkar (2003).

The analytical approach of the forced vibration technique is similar in principle to that described in Haan (2000) and Matsumoto (1996). Essentially, while driving the model in a prescribed sinusoidal motion, the pressure is measured on the top and bottom surfaces of the model in the streamwise direction. The pressure signals are integrated to obtain lift and moment time series. Phase relations between the motion (the angular and vertical position) and the aerodynamic forces (the lift and the moment) are estimated using a frequency domain approach. For an angular oscillation prescribed as:

$$\alpha = \alpha_0 \cos(\omega_\alpha t) \quad (2)$$

where α_0 is the amplitude of the angular oscillation and ω_α is the frequency of oscillation, the lift and the moment can be expressed as:

$$L = L_0 \cos(\omega_\alpha t - \phi_L)$$
$$M = M_0 \cos(\omega_\alpha t - \phi_M) \quad (3)$$

where L_0 and M_0 are the amplitudes of the fluctuating lift and moment, respectively, and ϕ_L and ϕ_M are the phase lags with respect to the angular position, α, of the lift and moment, respectively.

Given the above definitions, it can be shown that the flutter derivatives related to the pitching motion can be given as:

$$A_2^* = \frac{-M_0}{\alpha_0}\frac{\sin\phi_M}{qB^2K^2},\ A_3^* = \frac{M_0}{\alpha_0}\frac{\cos\phi_M}{qB^2K^2}$$

$$H_2^* = \frac{-L_0}{\alpha_0}\frac{\sin\phi_L}{qBK^2},\ H_3^* = \frac{L_0}{\alpha_0}\frac{\cos\phi_L}{qBK^2} \qquad (4)$$

where q is the dynamic pressure. Given a prescribed heaving motion such as $h = h_0\cos(\omega_h t)$ expressions for the heaving flutter derivatives, (A_1^*, A_4^*, H_1^*, H_4^*) can be derived as well. Both vertical lift, L, and heaving displacement, h, are defined as positive *downward*. To identify flutter derivatives for a range of reduced velocity values, the frequency of the motion of the model was held constant while the velocity of the tunnel was varied. In this paper, the pitching amplitude of B1 was 3 degrees and frequency of motion was 3.3 Hz. The heaving motion amplitude of Matsumoto's forced vibration tests of the rectangular sections with B/D=2 and 5 was 5 mm (Matsumoto, 1996).

4.0 CONSIDERATIONS ON UNCERTAINTY IN THE EXTRACTION OF FLUTTER DERIVATIVES THROUGH FORCED-VIBRATION METHOD

The phase angle between the model motion and the resulting self-excited forces plays a major role in the final value of the flutter derivatives, particularly for the A_2^* and H_2^* flutter derivatives. Contributions to phase angle uncertainty were estimated along with the corresponding influences to the flutter derivatives.

The phase angles ϕ_L and ϕ_M represent the phase lag between the maximum torsional displacement and the maximum value of lift and moment, respectively. These values were obtained by calculating a cross correlation function between the time series of angular position and lift (or moment). The time delay, τ, associated with the peak in the cross correlation function is the time delay from which the phase angle is calculated. The phase angle in degrees is calculated as $\phi = 360n\tau$, where n is the model oscillation frequency.

Three contributions to phase angle uncertainty were identified. First, the frequency response function of the pressure tubing has a finite uncertainty. Using a range of values for tubing length and sensor volume, the analytical expressions of Bergh and Tijdeman (1965) were used to calculate a range of tubing phase values at the body oscillation frequency. This range was used to estimate $u_{\phi_{tube}}$ to be $\pm 0.5°$ where $u_{\phi_{tube}}$ is the uncertainty in the phase resulting from tubing response.

The second contribution was from the finite sampling time of the pressure scanner. The pressure scanners sampling rate was 430 Hz (the maximum sustainable sampling rate). This means that the time delay calculations have a resolution of 1/430 seconds. This resolution was used as an estimate for $u_{\tau_{rate}}$, the uncertainty in the correlation time delay due to the finite sampling rate.

The third contribution originated from the non-simultaneous sampling of the pressure sensors. The pressure scanners interrogate each sensor sequentially, and therefore, there is a skew in time between one sensor sample and the next. The multiplexer scan rate is 50,000 Hz. The inter-channel scan rate then is found by dividing this rate by the 64 channels in the scanner, 781 Hz. The total delay between sampling the first and last channels is therefore 1/781 seconds. This value was used as the worst case estimate for $u_{\tau_{skew}}$, the uncertainty in the correlation time delay due to the non-simultaneous sampling of the pressure signals.

The impact of these *individual* contributions to flutter derivative values was estimated by calculating the flutter derivatives with these uncertainties added or subtracted from the phase values. The overall uncertainty in the phase angle was estimated in the conventional sum of squares approach shown below:

$$u_{\phi}^{2} = \left[u_{\phi_{tube}}^{2} + \left(\frac{\partial \phi}{\partial \tau} u_{\tau_{rate}} \right)^{2} + \left(\frac{\partial \phi}{\partial \tau} u_{\tau_{skew}} \right)^{2} \right] \quad (5)$$

where the $\frac{\partial \phi}{\partial \tau}$ derivative was estimated from the ϕ expression given earlier.

An example of uncertainty analysis associated with phase-lag effects can be found in Figures 7(a) to 7(d) for the B1 streamlined cross section, derived from ISU 1-DOF tests (torsional motion). Each plot is associated with a specific flutter derivative. These figures show the overall effects associated with the uncertainty in the definition of the phase angle (including tubing, sampling time and skew time). The reference ("Ref") curves (triangle symbol) were derived by averaging ten subsequent experimental realizations. In addition, upper ("Up") and lower ("Low") confidence bounds (square symbols) can also be seen; these corresponds to the error analysis associated with the overall phase angle effects. Figures analyzing the contribution associated with each individual component are available but were omitted for brevity. Moreover, a comparison with an equivalent set of free-vibration data is depicted.

One aspect of the uncertainty analysis that is immediately evident is the very low sensitivity of the A_3^* and H_3^* derivatives to phase uncertainty. In all cases, this sensitivity was negligible. This is due to the fact that the flutter derivatives are proportional to the cosine of the phase angle. A_2^* and H_2^* showed variations of as much as 20% and 50%, respectively, with these rather modest uncertainty estimates.

The other observation that can be made is that the sampling rate made the largest contribution to the uncertainty in the A_2^* and H_2^* flutter derivatives. Increasing the sampling rate appears to be the most effective way to reduce flutter derivative uncertainty.

5.0 FLUTTER DERIVATIVE COMPARISON

All eight flutter derivatives *H1*-H4** and *A1*-A4** for B1 that were extracted using the 2-DOF free vibration tests and the ILS method (Gan Chowdury and Sarkar, 2003, 2004) are plotted in Figures 6a and 6b for reference since these were used later for aeroelastic-instability sensitivity analysis. The comparison of *H1*, H4** and *A2*, A3** as extracted by 2-DOF Vertical-Torsional, Lateral-Vertical and Lateral-Torsional motions are shown in Figures 6c and 6d. Slight differences between the two sets are observed that could be because of the influence of amplitude of vibration of the second degree of freedom not directly associated with the direct flutter derivatives that are being compared. In other words, *H1** and *H4** are likely to be influenced by amplitudes of torsional and lateral motions while *A2** and *A3** are likely to be influenced by amplitudes of vertical and lateral motions.

As observed in Figure 7 and reported earlier (Sarkar et al., 2006), the flutter derivatives from free vibration and forced vibration of B1 generally compare well except it can be seen that *H2** falls below the lower confidence level of the forced-vibration test. One of the explanations that could be offered is that the data from the free vibration tests will also have an upper bound and a lower bound due to its sensitivity to various parameters including but not limited to number of degrees of freedom, sampling rate and sampling time, instrumentation and system identification method that were used to extract them. There is a good possibility that the upper bound of the free vibration data could overlap with the lower bound of the forced vibration data. The error analysis of the free vibration data has not been performed yet.

Figures 8 and 9 show some effect of amplitude on the flutter derivatives for the R2-1 and R5-1 bridge deck cases. It was observed for both the cross sections that the *H1** curve does not change between A=9 mm and 17 mm cases. In Figure 8, however, for the R2_1 and A=26 mm case the negative magnitudes of *H1** decreased with respect to the other two cases. Matsumoto's forced-vibration data with an amplitude of A=5 mm that is lower than the ISU cases is consistent with this observation. In this case, the negative magnitudes of *H1** are greater than the ISU cases. However, the higher positive values of this data set than those of the ISU cases can not be explained. The general trend of all the *H1** graphs is consistent including the zero crossing points. There is a clear trend in the ISU *H4** values for R2_1 case as shown in Figure 8b. The positive peak value of *H4** corresponding to different amplitudes does not change but the graphs tend to shift toward left for smaller amplitudes. The first zero crossing of the ISU, A=9 mm case compares well with Matsumoto's data. However, the positive peak values of ISU *H4** fall short of Matsumoto's positive peak value. This trend is consistent with those observed for *H1** in Figure 8a. In Figure 9, for R5_1 case, the comparison is generally good except some difference at higher reduced velocity in *H1**. The ISU data does not demonstrate any amplitude dependency in this case.

6.0 SINGLE AND COUPLED-MODE AEROELASTIC INSTABILITY SENSITIVITY ANALYSIS

A sensitivity study was conducted to understand the implications of the differences emerged during the experimental benchmark comparison on the wind-induced oscillation of long-span bridges. Two distinct cross sections were considered: Streamlined cross section with semi-circular fairings with B/D=14.3 (B1) and the bluff rectangular prism with B/D =2 (R2_1). Numerical simulations were carried out in order to identify the influence of the variations in the flutter derivatives, extracted from tests conducted either by different laboratories or under distinct operational conditions, on the critical velocity corresponding to the onset of dynamic instability. Both single-mode and coupled-mode aeroelastic vibration were analyzed (Scanlan and Tomko, 1971; Simiu and Scanlan, 1996).

Table 1 summarizes the different flutter derivative sets, which were separately considered during the simulations. For each cross section, the denomination refers to a particular experimental set, such as free (FV) or forced vibration (FFV), 2-DOF or 1-DOF, initial oscillation amplitude (A).

In relation to the B1 cross section, data derived from the tests conducted at ISU were exclusively employed, from which five simulation sets were extracted (Table 1): two sets corresponding to free-vibration tests exclusively (FV), and three sets associated with a combination of free and forced-vibration (FFV) experimental results.

With regard to the first two simulation scenarios sets associated with free-vibration tests, Figures 6(a) and 6(b) respectively show the H_q* and A_q* derivatives (q=1,..,4), labeled as set B1.A in Table 1 (2-DOF Vertical-Torsional tests). The second set (B1.B) was derived from the combination of the cross terms of B1.A and the direct terms related to two additional ISU sets (2-DOF L&T, L&V). In Figures 6(c) and 6(d) the comparison between sets B1.A and sets B1.B is presented (H_1*, H_4* and A_2*, A_3*, respectively) as a function of the reduced velocity, U/nB. Evident dissimilarities are limited to A_2* and A_3* in the reduced velocity range beyond 8.0, while they are much less pronounced for the other terms.

In relation to the simulation sets, Figures 7(a) to 7(d) present the B1-cross section derivatives H_2*, H_3*, A_2* and A_3* corresponding to the ISU 1-DOF forced-vibration experiments (torsional). In the figures free-vibration tests are included along with the sensitivity analysis to phase-angle errors, as indicated in Section 4.0. The corresponding simulation sets, derived from the derivatives in Figures 7 are indicated as B1.C to B1.E in Table 1; it must be observed that in the simulations flutter derivatives H_2*, H_3* and A_2*, A_3* were derived from a combination of the different curves related to the FFV sets (Figures 7), whereas the remaining curves were taken from the free-vibration data. A detailed description can be found in Table 1.

In relation to the R2_1 case, H_1*, H_4* data were exclusively considered, since this particular shape exhibits susceptibility to heaving-mode aeroelastic instability (single-mode galloping). Simulation sets included both 1-DOF ISU free-vibration wind tunnel tests, conducted at different amplitudes, and forced-vibration experimental sets reproduced from Matsumoto (1996). In Figures 8(a) and 8(b) the sets corresponding to H_1* and H_4* are respectively depicted as a function of U/nB.

Three long-span bridge configurations were analyzed. Multimode or single-mode analysis methods (e.g. Jones and Scanlan, 2001) were employed for the solution to the aeroelstic instability problem. Numerical procedures for aeroelastic simulations were derived from previous studies (Caracoglia, 2001) and adapted to the specific examples.

The mass and rotational moment of inertia of the deck/vibrating structure were simulated through a constant quantity per unit length (m_0 and I_0, respectively). Influence of the mode shape on the aeroelastic instability solution was neglected at this stage: mode shapes were postulated as simplified sinusoidal forms. Lateral modes were not considered.

The simulated structures are: Br1, a medium-span suspension-bridge (main span L=1200 m, deck width B=28 m, m_0=3.5×10^4 kg/m, deck torsional inertia I_0=4.4×10^6 kg×m^2/m); Br2, a short-span cable-stayed bridge (L=500 m, B=38 m, m_0=3.1×10^4 kg/m, I_0=2.8×10^6 kg×m^2/m); Br3, a long-span suspension bridge (L=3000m, B=60 m, m_0=3.1×10^4 kg/m, I_0=2.8×10^6 kg×m^2/m). In the case of Br1, for which the deck bending and torsional stiffness is predominant in comparison with those provided by the cables, the simulated modes (vertical and torsional) are symmetric, while these are skew-symmetric for Br2 and Br3.

In all the three cases a constant values of mechanical damping equal to 0.3% was considered, independently of the selected mode. Moreover, in the case of coupled-mode instability, perfect similarity between bending and torsional eigen-functions was considered. All these quantities were calibrated through the analysis of similar existing structures.

Table 2 summarizes the results of the coupled-mode simulations conducted on bridge types Br1, Br2, Br3 by considering the flutter derivative sets B1.A to B1.E; simulation scenarios (i) to (xv) were considered. For each scenario, the table shows the lowest critical eigen-value solution corresponding to the critical velocity of binary flutter (simple harmonic motion), based on two-mode analysis (Jones and Scanlan, 2001). In the table, the frequencies corresponding to the selected modes are also indicated, along with the critical reduced frequency (K_{crit}), flutter-mode frequency and velocity.

In relation to sets B1.A and B1.B, it must be observed that the variation between the two sets was exclusively simulated through direct terms (i.e., H_1*, H_4* and A_2*, A_3*), while differences in the cross-terms were not examined (Table 1). In contrast, both the direct (i.e., A_2*, A_3*) and the cross-terms (i.e., H_2*, H_3*) were considered in the sets from B1.D to B1.E.

Figure 10 shows the typical trajectories of the flutter real and imaginary solution branches. Flutter eigen-values (ratio between simple-harmonic-motion and torsional-mode frequencies, f_{shm}/f_{tors}) as a function of the reduced frequency ($K=\omega B/U$) are indicated for Br1 and set B1.A (a), Br3 and set B1.B (b). The two-mode flutter solution is highlighted in both cases. In all cases flutter seems to be dominated by the vertical mode because of the nature of the aeroelastic terms (streamlined cross section).

From the analysis of Table 2, differences of the order of few percent to a maximum of 8% (e.g., case (ii) vs. case (i)) can be observed between B1.A and B1.B for all three simulated bridge examples. Differences in the flutter speed are more evident for a medium-span bridge, at least for the investigated scenarios. The critical values of the reduced velocity can be located between 7.4 (Br3, case (xv)) and 33.4 (Br1, case (ii)). The latter case is clearly beyond the interval of measured U/nB (Figure 1) and the solution to the flutter problem was only possible through extrapolation of the experimental data associated with free-vibration tests.

In contrast, a disparity in the results was observed between the free and forced-vibration sets. As an example a 30% reduction in the flutter speed can be seen in Table 2 between case (iv) and (i) for Br 1, even though this result is affected by the fact that H_1*, H_4* and A_1*, A_4* are interpolated for U/nB>15. Similarly, a reduction in the flutter velocity was observed for Br2 and Br3 even though less significant (e.g., 13% reduction between (xiii) and (xi)).In all cases the discrepancy can be related to the measurements of H_2* (variations in both magnitude and sign, Figure 2(a)), responsible for the modal coupling during flutter.

Moreover, it can be concluded from Table 2 that the phase angle effect, typical of the sets derived through forced vibration, appears to be of secondary importance. A 3% maximum difference in the critical velocity was in general observed among sets B1.C, B1.D and B1.E (e.g., (ix) vs. (x) for Br2).

In the second part of the sensitivity study, heaving-mode aeroelastic instability was analyzed. This is a phenomenon similar to single-mode galloping, usually associated with inadequate aerodynamic characteristics of H_1* for bluff cross sections (Figure 8(a)). Results are summarized in Table 3. In this case bridge types Br1 and Br2 were only considered. Since a single-mode dynamic instability is damping driven, the initial selection of the structural damping value is important and had a direct effect on the assessment of the critical threshold. Nevertheless, relative differences among the investigated cases are of more relevance in this study since these are associated with the differences in measured H_1* and H_4* (Figure 8), derived under distinct operational conditions. The analysis of the data sets showed in fact a difference of the order of 30% in some cases between ISU and Matsumoto (1996), especially for H_1*. It was concluded that this effect in combination with an apparent shift of the different curves along the U/nB axis was responsible for the deviations in the critical velocities (Table 3), with variations between 5% and 20% for Br1, and 9% and 15% for Br2. The latter tends to show a more pronounced dissimilarity in comparison with others (Figure 8).

It must be observed that relative variations in the H_4* derivative are responsible for the differences in terms of critical frequency (equivalent added or subtracted mass aerodynamic component) in the simulations.

From the analysis of Table 3, it can be concluded that the effects on the heaving-mode instability, related to dissimilarities in the experimental extraction of flutter derivatives, cannot be neglected in the case of a bluff deck section. These considerations are strictly applicable to the selected case studies, and are affected by the evident simplifications introduced during the investigations. A more careful assessment, for example performed on real structures, is therefore required for a more general characterization of these aspects.

7.0 SUMMARY

This paper presents some recent results associated with a research activity focused on the comparison between different wind tunnel measurement techniques for the extraction of flutter derivatives for bridge aeroelastic analyses. This research was motivated by a benchmark study initiative promoted by Iowa State University, extended to the Japanese investigators within the scope of the UJNR cooperative research efforts.

In the first part of the study a systematic analysis of laboratory results was conducted; this included free and forced-vibration wind tunnel methods, currently routinely employed by researchers or designers. Data from a US laboratory under distinct operational conditions were analyzed and compared with literature results (Japan). Both streamlined and bluff deck sections were considered.

In particular, it was concluded that for bluff cross sections (rectangular prisms) differences emerged from the experimental data could be possibly associated with the effects of amplitude dependency of the aeroelastic terms. Moreover, a non-negligible dependence on the laboratory environment or the operational conditions was noticed, even for streamlined cross-sections. This fact also suggests that uncertainty (i.e., error) analyses (i.e., error estimation), as performed in this study for a set of derivatives derived through forced-vibration tests, should be carefully considered during wind tunnel operations and possibly included as a recommendation during preliminary bridge design.

In the second part of the research, a sensitivity study was performed on the implications of the perceived dissimilarities among flutter-derivative data sets on the aeroelastic instability of long-span bridges. A preliminary investigation was conducted on a restricted set of simulated bridges with simplified structural characteristics. Both bluff and streamlined deck cross sections were analyzed; single-mode (heaving) and coupled-mode instability for streamlined deck were considered. Results indicate that a variation of the order of ten to fifteen percent in the critical velocity was possible, either an increment or a decrement depending on the selected derivative set. This fact reaffirms the importance of uncertainty analysis of experimentally extracted flutter derivatives in the context of aeroelastic simulations. Moreover, effects such as phase-angle systematic errors, typical of the forced-vibration method, appear to be of secondary importance in comparison with other perceived dissimilarities (e.g., forced vs. free-vibration data sets), at least for streamlined sections. More investigation on perhaps more realistic or existing structures is necessary to fully quantify these implications and to provide a general guideline for designers or researchers.

8.0 ACKNOWLEDGMENTS

The contributions of technician, Bill Rickard, graduate students, Vasanth Balaramudu and Kevin Sehn, former graduate students, John Stronck and Arindam Gan Chowdhury, and many undergraduate students in the Department of Aerospace Engineering at Iowa State University, who contributed to this work, are gratefully acknowledged. We would like to acknowledge Dr. Hiroshi Sato at PWRI, Japan for providing insight to this work. The second author would like to acknowledge the partial support of Northeastern University, Office of the Provost, Research and Scholarship Development Fund (2006-2007), and start-up funding for new faculty members.

9.0 REFERENCES

Bergh, H., Tijdeman, H. (1965), “Theoretical and experimental results for the dynamic response of pressure measuring systems,” Nationaal Lucht en uimtevaartlaboratorium, NLR-TR F.238.

Caracoglia, L. (2001), “Wind-Structure Oscillations on Long-Span Suspension Bridges,” Ph.D. Dissertation, University of Trieste, Trieste, Italy.

Gan Chowdhury, A., Sarkar, P.P. (2003), “A New Technique for Identification of Eighteen Flutter Derivatives using a Three-Degree-of-Freedom Section Model,” Engineering Structures, v. 25, n. 14, 1763-1772.

Gan Chowdhury, A., Sarkar, P.P. (2004), “Identification of Eighteen Flutter Derivatives of an Airfoil and a Bridge Deck,” International Journal of Wind and Structures, Vol. 7, No. 3.

Haan, F.L., Jr. (2000), “The Effects of Turbulence on the Aerodynamics of Long-Span Bridges,” Ph.D. Dissertation, University of Notre Dame, Notre Dame, Indiana.

Jones, N.P., Scanlan, R.H. (2001), "Theory and full-bridge modeling of wind response of cable-supported bridges," Journal of Bridge Engineering, ASCE, v6, n6, 365-375.

Matsumoto, M., Kobayashi, Y., Shirato, H. (1996), "The influence of aerodynamic derivatives on flutter," Journal of Wind Engineering and Industrial Aerodynamics, 60, 227-239.

Matsumoto, M. (1996), “Aerodynamic Damping of Prisms,” Journal of Wind Engineering and Industrial Aerodynamics, v. 59, n. 2-3, 159-175.

Simiu, E., Scanlan, R.H. (1996), "Wind effects on structures," John Wiley and Sons, New York, NY, USA.

Sarkar, P.P., Haan, F.L., Stronck, J.M. and Balaramudu, V.K. (2006), “Forced and Free

Vibration Extraction of Flutter Derivatives: A Parametric Study-Based Comparison," Proc. Fourth UJNR Workshop on Wind Engineering, Tsukuba, Japan, July, 20-22.

Sarkar, P.P., Gan Chowdhury, A., Gardner, T.B. (2004), "A Novel Elastic Suspension System for Wind Tunnel Section Model Tests," Journal of Wind Engineering and Industrial Aerodynamics, v. 92, n. 1, 23-40.

Sato, H. (2004), Personal Communications, PWRI, Japan.

Scanlan, R.H. and Tomko, J.J. (1971), "Airfoil and Bridge Deck Flutter Derivatives," Journal of Engineering Mechanics, ASCE, v. 97, n. EM6, 1717-1737.

Table 1: Summary of the flutter-derivative data employed in the simulations (sections B1, R2_1).

Flutter Derivative Set	H_1*	H_2*	H_3*	H_4*	A_1*	A_2*	A_3*	A_4*
B1.A	ISU, FV-2 (V&T)	ISU, FV-2 (V&T)	ISU, FV-2 (V&T)	ISU, FV-2 (V&T)	ISU, FV-2 (V&T)	ISU, FV-2 (V&T)	ISU, FV-2 (V&T)	ISU, FV-2 (V&T)
B1.B	ISU, FV-2 (L&V)	ISU, FV-2 (V&T)	ISU, FV-2 (V&T)	ISU, FV-2 (L&V)	ISU, FV-2 (V&T)	ISU, FV-2 (L&T)	ISU, FV-2 (L&T)	ISU, FV-2 (V&T)
B1.C	ISU, FV-2 (V&T)	ISU, FFV-1 (T) "Ref"	ISU, FFV-1 (T) "Ref"	ISU, FV-2 (V&T)	ISU, FV-2 (V&T)	ISU, FFV-1 (T) "Ref"	ISU, FFV-1 (T) "Ref"	ISU, FV-2 (V&T)
B1.D	ISU, FV-2 (V&T)	ISU, FFV-1 (T) "Up"	ISU, FFV-1 (T) "Up"	ISU, FV-2 (V&T)	ISU, FV-2 (V&T)	ISU, FFV-1 (T) "Up"	ISU, FFV-1 (T) "Up"	ISU, FV-2 (V&T)
B1.E	ISU, FV-2 (V&T)	ISU, FFV-1 (T) "Low"	ISU, FFV-1 (T) "Low"	ISU, FV-2 (V&T)	ISU, FV-2 (V&T)	ISU, FFV-1 (T) "Low"	ISU, FFV-1 (T) "Low"	ISU, FV-2 (V&T)
R2_1.A09	ISU, FV-1 (V) A09	-	-	ISU, FV-1 (V) A09	-	-	-	-
R2_1.A17	ISU, FV-1 (V) A17	-	-	ISU, FV-1 (V) A17	-	-	-	-
R2_1.A26	ISU, FV-1 (V) A26	-	-	ISU, FV-1 (V) A26	-	-	-	-
R2_1.M	Matsumoto et al. (1996), FFV-1 (V)	-	-	Matsumoto et al. (1996), FFV-1 (V)	-	-	-	-

Notes: FV-1: free vibration (1-dof), FV-2: free vibration (2-dof), FFV-1: forced vibration (1-dof), V: vertical dof; T: torsional dof; L: lateral dof
Sections: B1 (streamlined cross section , B/D = 14.3); R2_1 (rectangular prism, B/D = 2). A: ampl. (A09=9, A17=17, A26=26mm)
Phase-angles: "Ref" (reference curve); "Up" (upper confidence level, Phi+dPhi in Figures 2); "Low" (lower confid. Level, Phi-dPhi in Figures. 2)

Table 2: Coupled-mode flutter simulations; sensitivity analyses.

Case Study (Bridge Type)	**Flutter Derivative Set**	**Vertical Mode Freq. (Hz)**	**Torsional Mode Freq. (Hz)**	**2Mode Flutter $K_{crit}=\omega B/U$**	**2Mode Flutter Freq. (Hz)**	**2Mode Flutter Speed (m/s)**
(i) Br1 (suspens., *L* =1200m)	B1.A	0.087	0.192	0.209	0.097	79.9
(ii) Br1	B1.B			0.188	0.094	85.9
(iii) Br1	B1.C			0.269	0.093	59.8
(iv) Br1	B1.D			0.266	0.093	60.3
(iv) Br1	B1.E			0.272	0.094	59.3
(vi) Br2 (cb.-stayed, *L* =500m)	B1.A	0.200	0.500	0.447	0.203	108.2
(vii) Br2	B1.B			0.449	0.202	107.7
(viii) Br2	B1.C			0.499	0.204	97.5
(ix) Br2	B1.D			0.493	0.203	98.5
(x) Br2	B1.E			0.505	0.204	96.6
(xi) Br3 (suspens., *L* =3000m)	B1.A	0.061	0.079	0.676	0.058	32.2
(xii) Br3	B1.B			0.721	0.059	30.9
(xiii) Br3	B1.C			0.848	0.060	26.7
(xiv) Br3	B1.D			0.833	0.060	27.2
(xv) Br3	B1.E			0.844	0.060	26.9

Table 3: Heaving-mode instability simulations; sensitivity analyses.

Case Study (Bridge Type)	**Flutter Derivative Set**	**Vertical Mode Freq. (Hz)**	**Heaving-Mode $K_{crit}=\omega B/U$**	**Heaving-Mode $U_{R,crit}$ (1)**	**Heaving-Mode Crit. Freq. (Hz)**	**Heaving-Mode Crit. Speed (m/s)**
(i) Br1 (suspens., *L* =1200m)	R2_1.A09	0.087	0.61	10.36	0.078	22.1
(ii) Br1	R2_1.A17		0.55	11.35	0.077	24.1
(iii) Br1	R2_1.A26		0.52	12.13	0.077	25.5
(iv) Br1	R2_1.M		0.57	11.05	0.069	20.9
(v) Br2 (cb.-stayed, *L* =500m)	R2_1.A09	0.200	0.61	10.34	0.160	62.9
(vi) Br2	R2_1.A17		0.55	11.32	0.159	68.5
(vii) Br2	R2_1.A26		0.52	12.07	0.156	71.8
(viii) Br2	R2_1.M		0.57	11.04	0.132	55.3

Note (1): $U_{R,crit}=2\pi/_{Kcrit}$

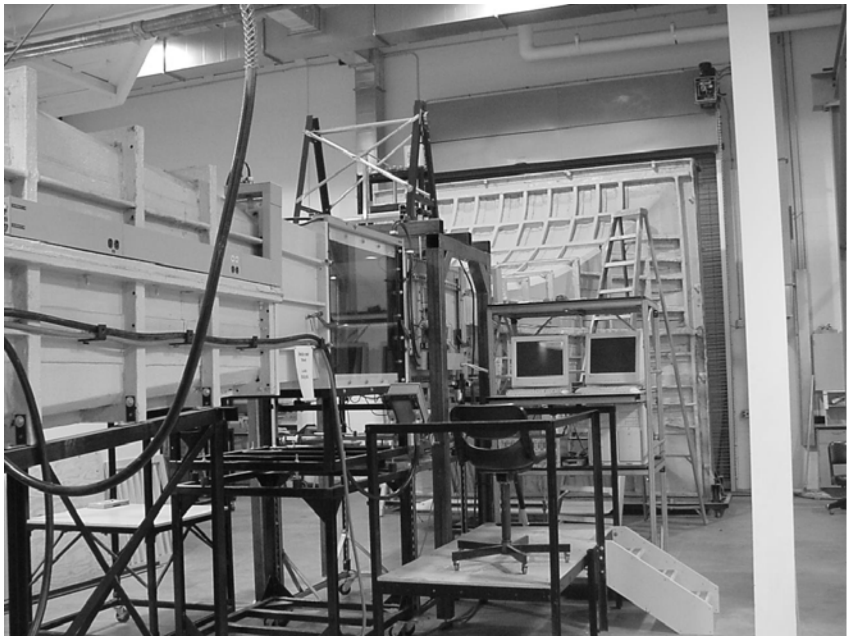

Figure 1: Bill James Wind Tunnel with forced-oscillation system installed on overhead frame.

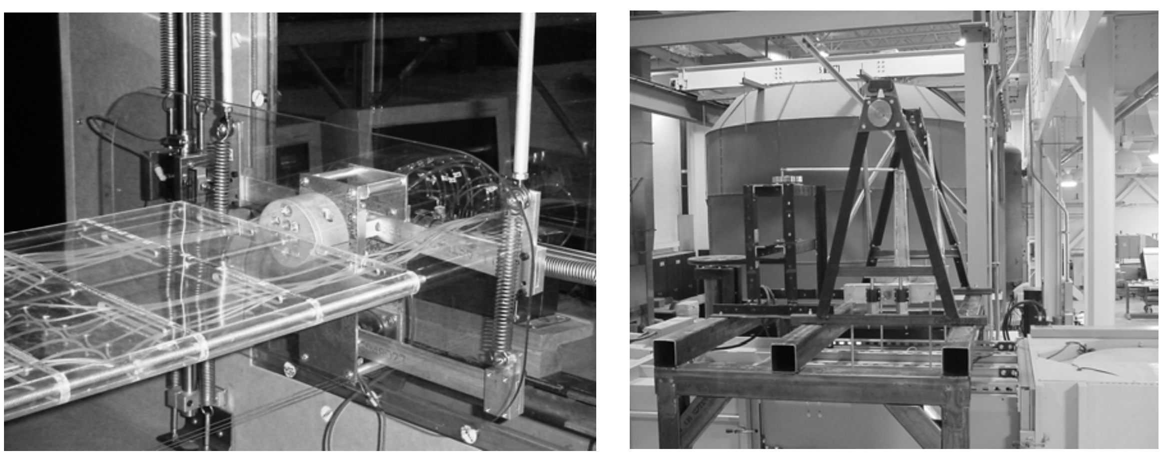

Figure 2: B1 Bridge model and model support structure (left) showing both spring mounts for free vibration and the push rods for forced vibration and forced oscillation system (right) showing motor and rocker arms used to actuate the push rods.

Figure 3: Free-vibration suspension system initial condition apparatus.

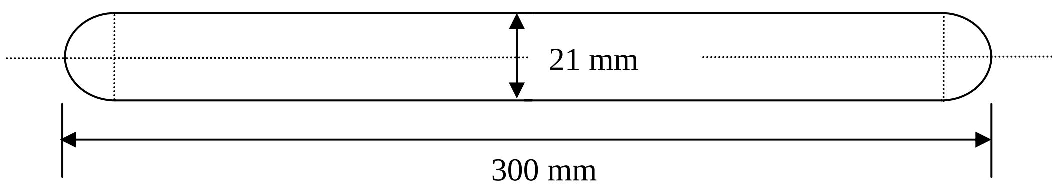

Figure 4: Diagram of streamlined bridge deck model, B1, used for comparing free and forced vibration methods of acquiring flutter derivatives in the Bill James Wind Tunnel at ISU.

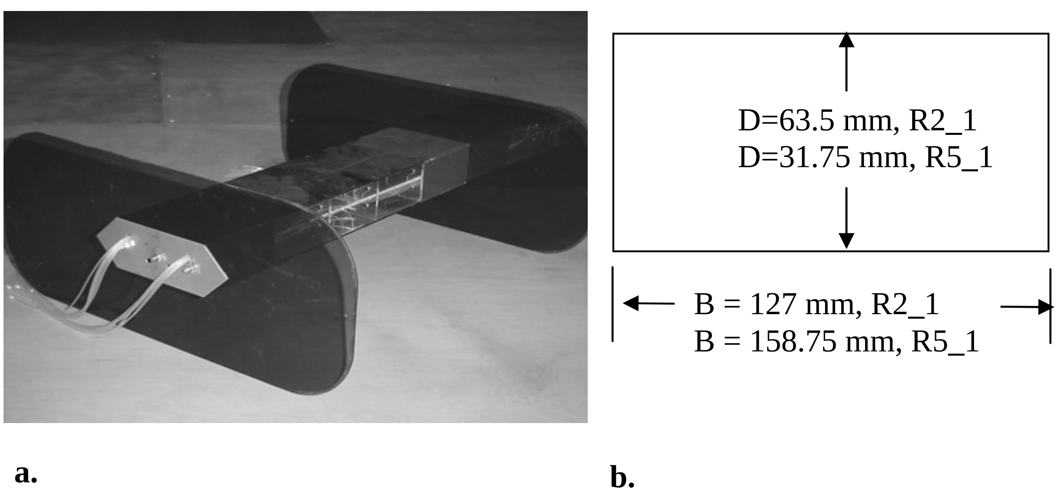

Figure 5: a. Rectangular box girder section model, R2_1, b. Dimensions for the B/D =2 (R2_1) and B/D =5 (R5_1) models.

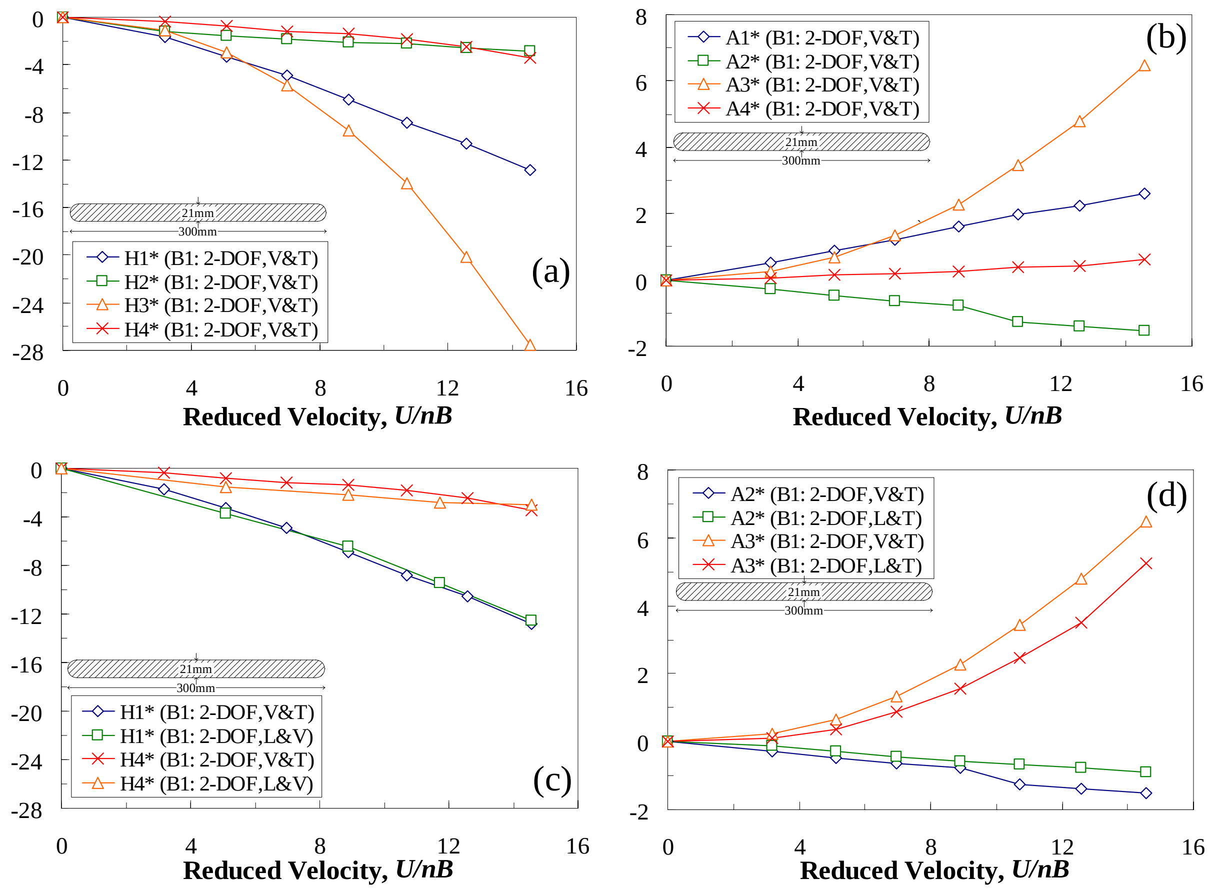

Figure 6: Flutter derivatives of B1 (ISU free-vibration tests) employed in the coupled-mode flutter simulations. H_q* (a) and A_q* (b) derivative set (q=1,..,4) corresponds to B1.A (2-DOF Vertical-Torsional); (c) H_1*, H_4* comparison between sets B1.A and B1.B (2-DOF Lateral & Vertical); (c) A_2*, A_3* comparison between sets B1.A and B1.B (2-DOF Lateral & Torsional).

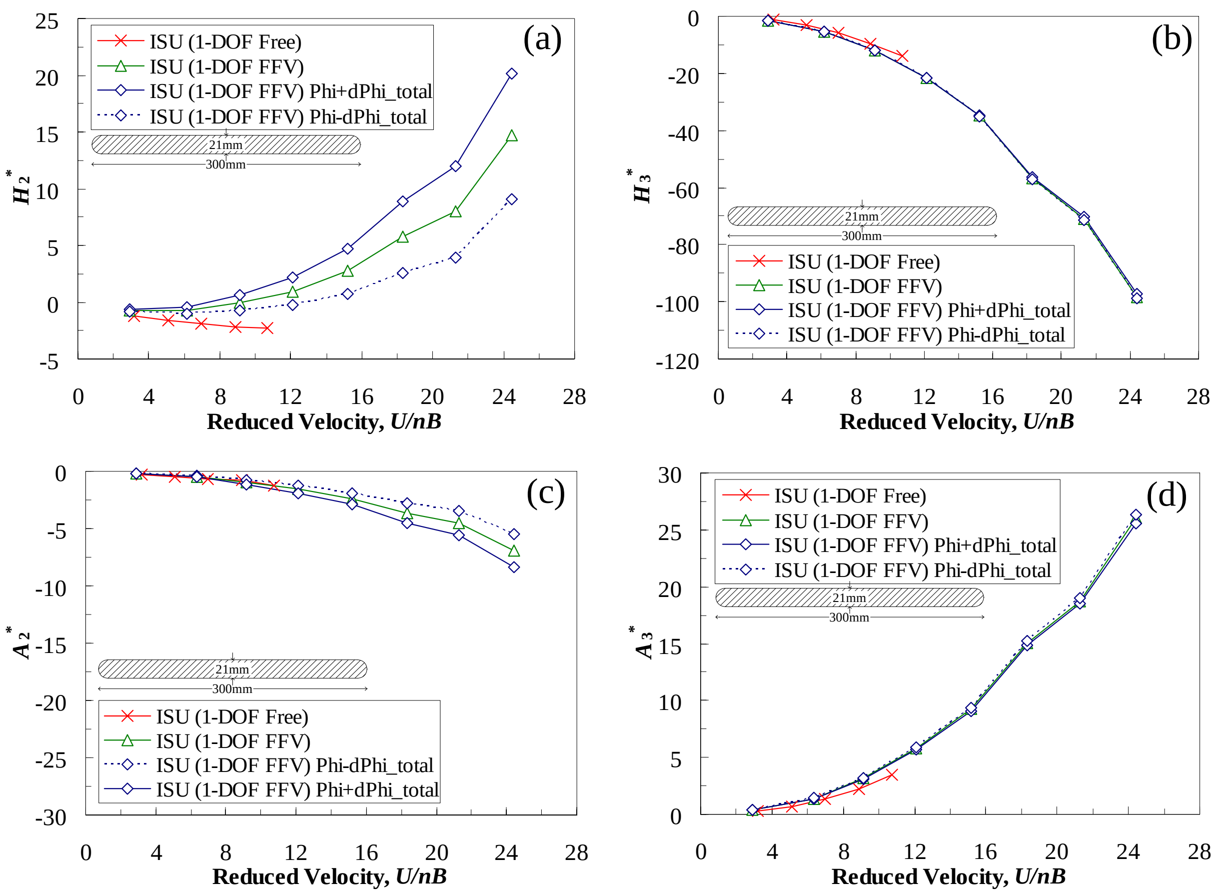

Figure 7: Flutter derivatives of B1 (ISU 1-DOF forced-vibration tests, Torsional or 1-DOF FFV), including sensitivity analysis to determine phase-angle errors. (a) H_2*, (b) H_3*, (c) A_2*, (d) A_3*. "(1-DOF FFV)": reference curves; "(1-DOF FFV) Phi+dPhi_total" upper confidence level; "(1-DOF FFV) Phi-dPhi_total" lower confidence level, and their comparison with the 1-DOF free vibration data.

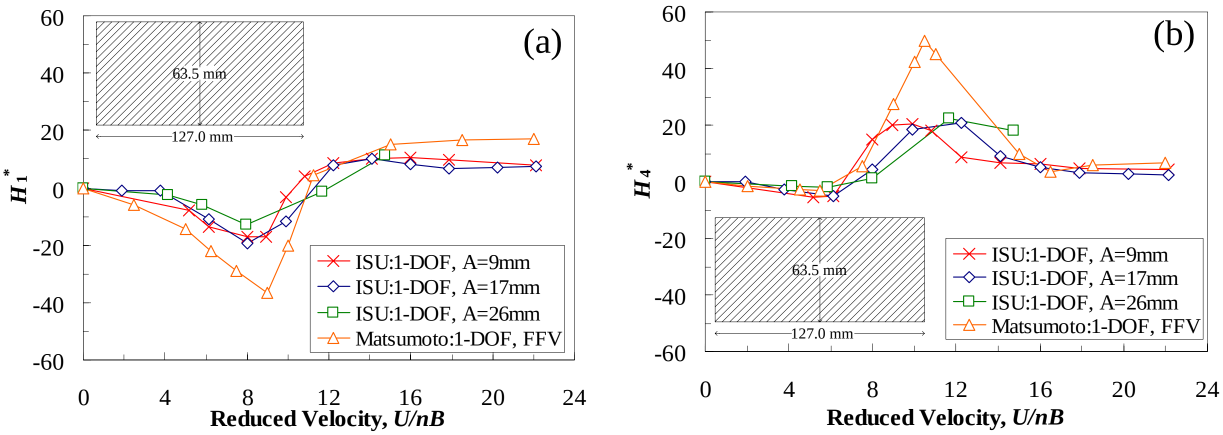

Figure 8: H_1* (a) and H_4* (b) flutter derivatives of the rectangular cross section R2_1 (AR 2:1) employed in the aeroelastic simulations. Comparison between the ISU 1-DOF vertical free-vibration experiments (A: initial amplitude) and the data reproduced from Matsumoto (1996), (FFV: forced vibration).

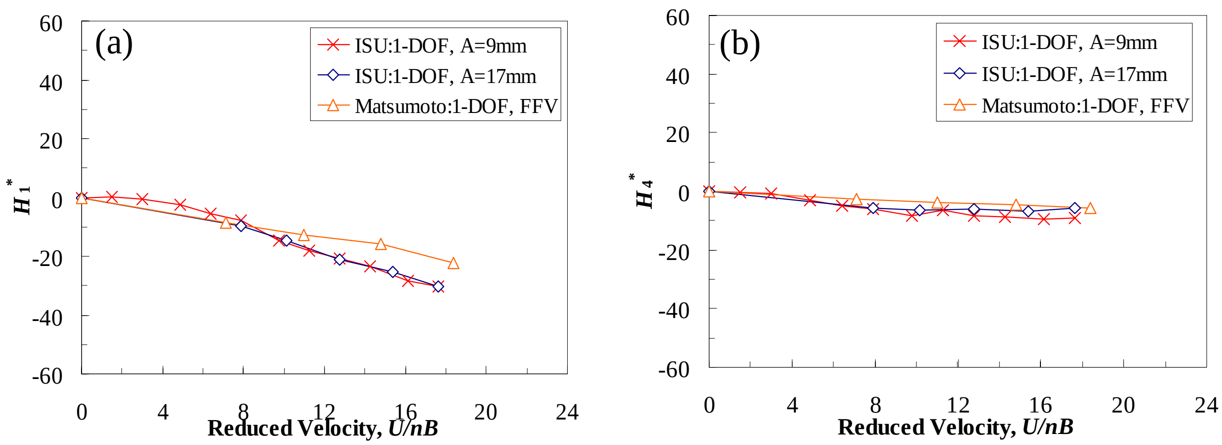

Figure 9: H_1* (a) and H_4* (b) flutter derivatives of the rectangular cross section R5_1 (AR 5:1). Comparison between the ISU 1-DOF vertical free-vibration experiments (A: initial amplitude) and the data reproduced from Matsumoto (1996), (FFV: forced vibration).

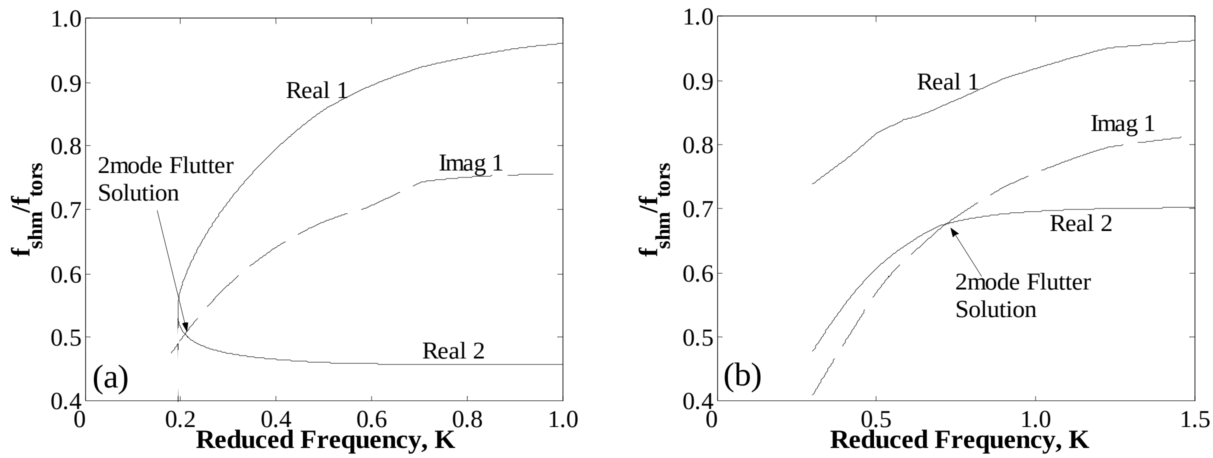

Figure 10: Example of coupled-mode flutter real and imaginary solution branches. Flutter eigen-value (ratio between simple-harmonic-motion and torsional-mode frequencies, f_{shm}/f_{tors}) as a function of the reduced frequency ($K=\omega B/U$). (a) Bridge type Br1, derivative set B1.A; (b) bridge type Br3, derivative set B1.B.